Magnetization distribution in the ordered $Fe_{72}Pt_{28}$ Invar alloy

2004 J. Phys.: Condens. Matter 16 5349

(http://iopscience.iop.org/0953-8984/16/29/024)

INSTITUTE OF PHYSICS PUBLISHING JOURNAL OF PHYSICS: CONDENSED MATTER

J. Phys.: Condens. Matter **16** (2004) 5349–5358 PII: S0953-8984(04)81087-7

Magnetization distribution in the ordered $Fe_{72}Pt_{28}$ Invar alloy

P J Brown[1,2], T Chatterji[1], J Kästner[3] and K R A Ziebeck[2]

[1] Institut Laue-Langevin, BP156 F 38042 Cedex, France
[2] Department of Physics, Loughborough University, Loughborough LE11 3TU, UK
[3] Institut für Physik, Experimentalphysik, AG Farle, Universität Duisburg-Essen, 47048 Duisburg, Germany

Received 24 May 2004
Published 9 July 2004
Online at stacks.iop.org/JPhysCM/16/5349
doi:10.1088/0953-8984/16/29/024

Abstract

The distribution of magnetization in the ordered Invar alloy $Fe_{72}Pt_{28}$ has been studied as a function of temperature in the range 100–520 K using polarized neutron diffraction. The temperature range covers both the Invar region and the paramagnetic regime in which the thermal expansion has normal Grüneisen behaviour. The polarized neutron data have been analysed in terms of localized iron 3d and Pt 5d moments allowing local anisotropy of the magnetization distribution on the Fe atoms. The results suggest that the Pt atoms carry a small negative moment ($\approx 0.3\ \mu_B$) in the magnetically ordered state. The fraction of unpaired electrons with e_g symmetry is approximately 48% and does not change with temperature. This is in contradiction to models of the Invar effect which invoke the thermal population of two states with a different number of e_g and t_{2g} carriers.

1. Introduction

The Invar effect was first discovered some 100 years ago in iron–nickel alloys [1]. The face centred cubic (fcc) alloys of iron and nickel containing roughly 35% of nickel ($Fe_{65}Ni_{35}$) have an almost zero thermal expansion coefficient over a broad temperature range. The Invar effect disappears above the Curie temperature, which suggests that the magnetic properties must in some way offset the normal lattice expansion and this premise is the foundation for most explanations given for the effect. Most theories derive from the original two-state Weiss model [2] which attributes the effect to thermally induced transitions between states with high moment and volume and others of closely similar energy having low moments and low atomic volumes. The Weiss model has been given a quantum mechanical basis by band structure calculations [4, 5]. The energy difference between the two states was shown to be a function of the electron concentration and to vanish at $e/a = 8.6$. A rather different origin for the

Invar effect is suggested by cluster calculations for Fe–Ni alloys [3]; these show that for a narrow range of nickel concentration there is a near overlap at the Fermi energy between majority spin states of strongly antibonding character and minority spin states of non-bonding character. Thermal population of the non-bonding states at the expense of the antibonding ones increases the bond strength which counteracts the vibrational lattice expansion. The band structure calculations of Entel [6] provide a basis for either or both of these mechanisms. Zero-field calculations made as a function of atomic volume give low moment (LM) solutions for small atomic volumes and high moment (HM) solutions for large atomic volumes. For Fe–Ni Invar the HM state is the ground state and the LM state is accessible with thermal energies. The symmetries of the electrons giving rise to the magnetization are different for the HM and LM solutions. Thermally induced excitation of the LM at the expense of the HM solution should lead to a steady decrease with increasing temperature of the atomic volume and a corresponding increase in the e_g character of the spin density. A polarized neutron study of the temperature variation of the magnetization distribution in $Fe_{65}Ni_{35}$ failed to show any such change in symmetry [7]. The magnetic form factor was found to be essentially independent of temperature in the range 100–600 K.

A number of other alloys have been found to exhibit the Invar effect; they always contain at least one transition metal and have e/a in the range 8.5–8.7. The Invar property is almost always associated with ferromagnetism and very often with alloys which like $Fe_{65}Ni_{35}$ are close to a martensitic instability. Fe_3Pt is one such alloy; it orders with the $L1_2$ (Cu_3Au) structure, but is unstable at the nominal Fe_3Pt composition at low temperatures. $Fe_{72}Pt_{28}$, the composition studied here, is stable against the martensitic transformation in both the ordered, $L1_2$, and disordered states. Studies of magnetization and thermal expansion of $Fe_{72}Pt_{28}$ [8] give Curie temperatures of 500 and 371 K for the ordered and disordered states respectively. The thermal expansion in both states increases slowly from low temperatures to a shallow maximum around 300 K then decreases to a minimum near T_C; at higher temperatures it recovers the normal Grüneisen behaviour. Inelastic neutron scattering studies [9, 10] demonstrate pronounced softening of the $\{\zeta\zeta 0\}$ TA modes at temperatures below T_C in the ordered state which is much less marked in the disordered crystal. Early studies [11] suggested that, as in $Fe_{65}Ni_{35}$, the spin-wave stiffness obtained from inelastic neutron scattering measurements was much greater than that derived from the temperature dependence of the magnetization. This is confirmed by the more recent measurements on both ordered and disordered $Fe_{72}Pt_{28}$ [12]: the spin-wave dispersion gave $D(0) = 107(1)$ and 98(4) meV Å^2 for the ordered and disordered alloys respectively, whereas the values obtained from magnetization measurements were 89 and 74 meV Å^2. This shows that, as in $Fe_{65}Ni_{35}$ Invar, some magnetic excitation besides spin waves must be present. Further inelastic neutron scattering experiments on $Fe_{72}Pt_{28}$ [13] have demonstrated the presence of a 'forbidden' mode: an excitation with the dispersion of the $\{\zeta 00\}$ TA phonon, but seen in longitudinal scans in the [100] direction. A similar mode, observed in $Fe_{65}Ni_{35}$ [14], has been shown to be of primarily magnetic origin.

An early polarized neutron study of the magnetic form factor of the ordered Fe_3Pt alloy at ambient temperature [15] gave moments of 2.03(2) for Fe and 0.36(8) for Pt. Because of the near equality of the scattering lengths of Fe and Pt only the fundamental reflections could be measured; hence the interpretation of the results depends heavily on assumptions made in the analysis. In order to verify whether the temperature invariance of the Fe form factor found in the disordered $Fe_{65}Ni_{35}$ alloy holds also for an ordered Invar alloy we have carried out a polarized neutron study of $Fe_{72}Pt_{28}$ in the temperature range 100–520 K, using a sample containing iron enriched with the low scattering length ^{57}Fe isotope, to enable measurement of superlattice as well as fundamental reflections.

2. Experimental details

2.1. Material

Neutron scattering studies of iron platinum alloys are difficult because of the close similarity of the two scattering lengths. For the present experiment we have used a sample prepared from iron isotopically enriched with 28.2 at.% commercial ^{57}Fe. To obtain a highly ordered state, the crystal was heat treated in a high purity argon atmosphere for 1 h at 730 °C, 3 d at 650 °C, 7 d at 600 °C, 7 d at 550 °C and 1 d at each of ten steps of −10 °C from 540 to 450 °C. The Bragg–Williams long range order parameter $S = 0.90(3)$ was estimated from magnetization measurements and by reference to x-ray data obtained from other samples which had similar compositions and heat treatments. If the sites at the cell origin are labelled A and those on the face centres B then, using the Bragg–Williams notation, when $S = 0.9$ the fraction r_A of A sites occupied by Pt is 0.955 and the fraction r_B of B sites occupied by Fe is 0.945. Taking the scattering length of natural iron as 9.45 fm and assuming that the commercial ^{57}Fe contains 92.52 at.% of ^{57}Fe with the scattering length 2.3 fm, the scattering length expected for Fe in the crystal is 7.53 fm compared to 9.6 fm for Pt. The crystal used was in the form of a pillar, $2 \times 2 \times 5$ mm^3, elongated parallel to $\langle 110 \rangle$. The magnetization at 100 K and 4 T measured with a squid magnetometer was 121.3(5) emu g^{-1} which corresponds to a magnetic moment of 8.28 μ_B/cell.

2.2. Polarized neutron experiments

The polarized neutron diffractometer D3 at the ILL was used in two series of experiments. In the first the crystal was mounted with its long axis vertical and parallel to the field direction of a 4.6 T superconducting magnet. The sample temperature was maintained at 100 K throughout. During this experiment the ILL hot source was operating and, in order to estimate the extinction in the crystal, the measurements were made at three wavelengths: 0.84, 0.51 and 0.42 Å. Resonant filters: 0.5 mm Er and 0.2 mm Rh were used at 0.84 and 0.51 Å to reduce the half-wavelength contamination. The polarized neutron flipping ratios of all accessible reflections hhl with $\sin\theta/\lambda < 1.0$ Å^{-1} were measured at all three wavelengths. Measurements of some $h, h-1, l$ reflections were also made at the two longer wavelengths. For the second series of measurements the hot source was not in operation so measurements were restricted to 0.84 and no filter was used. For these experiments the crystal was mounted in the special high temperature insert for the 10 T superconducting magnet and measurements of the polarization ratios of as many reflections as possible from the same set of reflections were made at temperatures of 520 and 300 K in a field of 9.5 T.

2.3. Unpolarized neutron experiments

Integrated intensity measurements were made on the same crystal with unpolarized neutrons in order to determine the temperature factors, and in particular whether any difference develops between the factors associated with the two sites, at high temperatures. The data were collected using the four-circle diffractometer D9 at the ILL. The incident neutron wavelength was 0.84 Å and measurements of all accessible reflections with $\sin\theta/\lambda < 1.0$ Å^{-1} were made at 100, 300 and 450 K. For the two lower temperature experiments the sample was mounted on the cold stage of a two-stage Displex refrigerator mounted on the ϕ circle; the temperature was controlled using a resistive heater. For the 450 K measurement a four-circle resistive furnace was used.

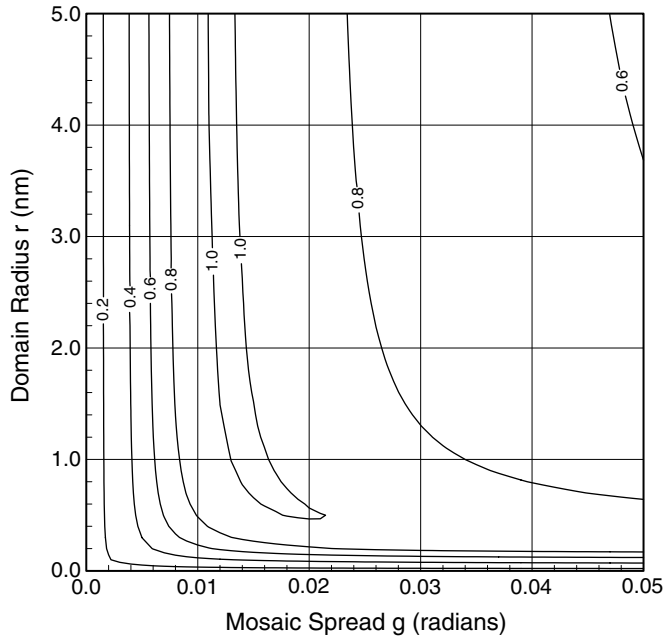

Figure 1. The inverse spread function of γ values calculated from the flipping ratios of low angle fundamental reflections from $Fe_{72}Pt_{28}$ measured at three different wavelengths, plotted as a function of the domain radius and mosaic spread parameters of the Becker–Coppens model for secondary extinction [16].

3. Analysis of the data

3.1. Extinction

The strong low angle reflections from $Fe_{72}Pt_{28}$ have flipping ratios which are significantly different from unity and for this case the degree of extinction can be determined with greater precision from the wavelength dependence of these ratios than from the wavelength dependence of the integrated intensities. The polarization ratios measured for the seven lowest angle fundamental reflections have been used to derive the two extinction parameters (domain radius and mosaic spread) of the Becker–Coppens model for secondary extinction [16]. For each reflection and any given pair of extinction parameters, the ratios γ between the magnetic and nuclear structure factors can be calculated from the polarization ratios for each of the three wavelengths. These should not be significantly different if the extinction is correctly modelled. The extinction parameters have been varied so as to find a minimum in the sum over reflections of the mean square deviations of the three γs from the mean for each reflection. This procedure is illustrated in figure 1 which shows a contour plot of the inverse of this quantity as a function of the two extinction parameters. It can be seen that there is a narrow ridge for mosaic spread $g = 0.013$ rad giving almost the same goodness of fit for all values of the domain radius $r > 4$ nm. This is the behaviour expected in the Becker–Coppens model when $g \gg \lambda/r$: the extinction is determined by the mosaic spread g only. The value $r = 1000$ nm was used in all further analysis.

3.2. Half-wavelength contamination

The difference between the Fe and Pt scattering lengths is not large, even for this isotopically enriched sample, and so the ratio between the intensities of the fundamental (*hkl* all even or all odd) and the superlattice (*hkl* mixed) reflections is very high ≈300. The effects of half-wavelength contamination of the incident neutron beam, even when filtered, are therefore important, particularly in the polarization ratios measured whilst the hot source was working. The half-wavelength contamination on D3 is due to the strong scattering of the 222 reflection from the Cu_2MnAl monochromator; this reflection is of primarily nuclear origin and so the half-wavelength neutrons are effectively unpolarized. The expression for the flipping ratio R of a reflection with scattering vector k, allowing for half-wavelength contamination but neglecting extinction, can be written as

$$R(k) = \frac{(1+\gamma^2+2P^+\gamma)+C/2Q}{(1+\gamma^2+2P^-\gamma)+C/2Q} \tag{1}$$

where $\gamma = F_M(k)/F_N(k)$ is the ratio between the magnetic and nuclear structure factors, P^+ and P^- are the beam polarizations with the flipper on and off respectively, C is the fraction of half-wavelength neutrons in the beam and $Q = 8|F_N(k)|^2/|F_N(2k)|^2$ is the ratio of the scattering powers of the reflections at k and $2k$. This equation has turning points ($dR/d\gamma = 0$) when $\gamma^2 = 1 + C/2Q$. R is a maximum if γ is positive and a minimum if it is negative, the extremal value depending strongly on C/Q. For the superlattice reflections of $Fe_{72}Pt_{28}$, γ is negative and the flipping ratios measured for the superlattice reflections pass through the minimum with increasing scattering angle as the magnetic scattering at first exceeds, then equals and finally falls below the nuclear scattering. The value of R at the minimum can be used to determine the half-wavelength contamination, using the known values of P^+ and P^-. To do this it was assumed that the angular dependence of the magnetic scattering in these low angle reflections can be approximated by a spherical Fe 3d form factor. Then $\gamma = \mu f(k)/N(k)$ and the flipping ratios of the low angle superlattice reflections can be fitted by varying the value of μ and the values of C/Q for the three wavelengths.

Although the nuclear scattering from the superlattice reflections is weak, the magnetic contribution to the lower angle ones may be strong enough to give rise to significant extinction. In such cases equation (1) must be rewritten to include the extinction factors y_k^+, y_k^- for the reflection at k for neutrons polarized parallel and antiparallel to the field, as well as the factor y_{2k} for scattering of half-wavelength neutrons by the reflection at $2k$. Then

$$R(k) = \frac{(y_k^+ + y_k^-)(1+\gamma^2+2P^+\gamma)+2P(y_k^+ - y_k^-)(P^+(1+\gamma^2)+2\gamma)+C/Qy_{2k}}{(y_k^+ + y_k^-)(1+\gamma^2+2P^-\gamma)+2P(y_k^+ - y_k^-)(P^-(1+\gamma^2)+2\gamma)+C/Qy_{2k}}. \tag{2}$$

The fractions C of half-wavelength neutrons were determined by making a least squares fit of the R values for the six lowest angle superlattice reflections measured in each set to equation (2) using the extinction parameters determined previously.

3.3. Temperature factors

The integrated intensities of all reflections measured at each of the two temperatures were averaged over equivalent reflections and then used in a least squares refinement to obtain the isotropic temperature factors. The half-wavelength contamination on D9 (with no hot source), estimated from the intensity at the $\frac{1}{2}\frac{1}{2}\frac{3}{2}$ position, was found to be negligible. The extinction was evaluated using the parameters determined above and its validity is confirmed by the quality of the refinement. At 300 K the material is ferromagnetic: the magnetic scattering was modelled using a spherical Fe 3d form factor and moments at the two sites of 2.4 and 0.15 μ_B

estimated from a preliminary analysis of the polarized neutron data. The refinement gave isotropic temperature factors 0.27(4) Å^2 for Fe and 0.18(4) Å^2 for Pt with an agreement factor $R = 0.032$. At 450 K the magnetic contribution to the integrated intensities can be neglected; the temperature factors obtained were 0.52 and 0.53(4) Å^2 for Fe and Pt respectively with an agreement factor $R = 0.040$.

3.4. Determination of the magnetic structure factors

The extinction parameters, half-wavelength fractions and temperature factors were used to obtain the magnetic structure factors F_M from equation (2) modified to allow for scattering vectors inclined at angle $\rho \neq 90°$ to the polarization direction:

$$R(k) = \frac{(y_k^+ + y_k^-)(1 + \gamma'^2 + 2P^+\gamma'') + 2P(y_k^+ - y_k^-)(P^+(1 + \gamma'^2) + 2\gamma'') + C/Qy_{2k}}{(y_k^+ + y_k^-)(1 + \gamma'^2 + 2P^-\gamma'') + 2P(y_k^+ - y_k^-)(P^-(1 + \gamma'^2) + 2\gamma'') + C/Qy_{2k}} \tag{3}$$

where $\gamma' = \gamma \cos\rho$ and $\gamma'' = \gamma \cos^2\rho$.

The magnetic structure factors for equivalent reflections measured at the same temperature and wavelength were averaged together and their standard deviations estimated from the deviations of individual measurements from the mean. For a preliminary analysis the magnetic structure factors obtained in this way were used to fit the parameters of a simple model of the magnetization distribution made from a sum of spherical magnetization distributions centred on the atomic sites. In this model the magnetic structure factors $F_M(\mathbf{k})$ are written as

$$F_M(hkl) = \mu_{Pt} r_A \langle j_0\rangle_{Pt} + \mu_{FeA}(1 - r_A)\langle j_0\rangle_{Fe} + 3r_B(\mu_{FeB}\langle j_0\rangle_{Fe} + s\langle j_2\rangle_{Fe})$$
$$\text{for } h, k, l \text{ all even or all odd} \tag{4}$$

$$F_M(hkl) = \mu_{Pt} r_A \langle j_0\rangle_{Pt} + \mu_{FeA}(1 - r_A)\langle j_0\rangle_{Fe} - r_B(\mu_{FeB}\langle j_0\rangle_{Fe} + s\langle j_2\rangle_{Fe})$$
$$\text{for } h, k, l \text{ mixed even and odd.} \tag{5}$$

In this equation μ_{Pt} and μ_{FeA} are respectively the magnetic moments of Pt and Fe atoms at the A sites, μ_{FeB} is the magnetic moment of Fe at the B sites; any scattering from Pt moments at the B sites can be neglected. $\langle j_0\rangle_{Pt}$, $\langle j_0\rangle_{Fe}$ and $\langle j_2\rangle_{Fe}$ are the form factors for Pt 5d and Fe 3d electrons. The term $s\langle j_2\rangle_{Fe}$ allows some flexibility in the shape of the spherical Fe form factor. It is possible to distinguish μ_{Pt} from μ_{FeA} because the shapes of the two form factors are very different as illustrated in figure 2. The results of the least squares fit are given in the first column of table 1. The high value obtained for μ_{FeA} is not realistic and shows that at least one of the assumptions made in the analysis cannot be valid. The analysis, and in particular the value of the magnetization at the A sites, is critically dependent on the calculated intensity ratio between the fundamental and superlattice reflections. This depends both on the order parameter S and on the value (7.53 fm) assumed for the scattering length of Fe. To determine the extent of this dependence the whole analysis procedure was repeated with several different values of these parameters. Decreasing S so that more Pt sites were occupied by Fe atoms still gave an unphysically large value of μ_{FeA}, 5.1 μ_B for $S = 0.8$. Increasing S increased μ_{FeA} because r_A became vanishingly small, whilst the 3d moment at the A site only decreased slowly. The only way in which μ_{FeA} could be reduced to a reasonable value was by decreasing the nominal scattering length of Fe to 0.72 and leaving $S = 0.9$. The results derived using different assumptions are summarized in table 1.

The values $b_{Fe} = 7.2$ fm $S = 0.9$ and the mosaic spread parameter $g = 0.014$ rad, together with the temperature factors derived from the integrated intensity measurements, were used to derive the magnetic structure factors from the flipping ratios at each of the three measurement temperatures: 520, 300 and 100 K. The complete list of unique structure factors together with

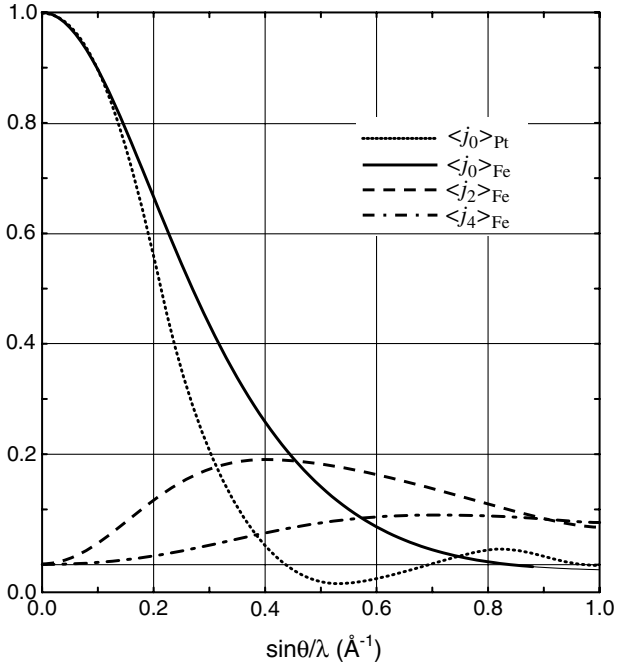

Figure 2. Iron 3d and platinum 5d form factors used in least squares fits of the magnetic structure factors. The iron form factors are taken from [17] and the platinum one is a spherical average of those given in [18].

Table 1. Parameters derived in analyses of the polarized neutron flipping ratios from $Fe_{72}Pt_{28}$ measured at 100 K using different values for the short range order parameter S and the scattering length of Fe (b_{Fe}). g is the mosaic spread parameter of the extinction model and the C parameters are those defined in equation (2).

	S	0.90	0.80	0.96	0.90	0.90
Parameter	b_{Fe} (fm)	7.53	7.53	7.53	8.0	7.2
g (rad)		0.013	0.012	0.013	0.012	0.014
C at 0.84 Å		0.017(7)	0.014(6)	0.017(6)	0.007(3)	0.018(10)
C at 0.51 Å		0.031(15)	0.022(10)	0.037(20)	0.014(8)	0.033(19)
C at 0.42 Å		0.001(16)	0.000(19)	0.002(23)	0.001(9)	0.002(10)
μ_{FeB} (μ_B)		91(10)	2.89(8)	2.9(8)	2.83(8)	2.95(8)
μ_{PtA} (μ_B)		−0.31(14)	−0.28(16)	−0.24(12)	−0.23(16)	−0.24(16)
μ_{FeA} (μ_B)		10(2)	5.1(8)	∞[a]	21.6(1.9)	0.7(2.0)
R[b]		0.087	0.087	0.087	0.092	0.068

[a] With $S = 0.96$ $r_A = 0$ the 3d moment determined for the A site was 0.25(11) μ_B.
[b] $R = \Sigma_i(|F_i^{obs} - F_i^{calc}|)/\Sigma_i|F_i^{obs}|$ where i labels the observations.

their standard deviations, estimated from the deviations of equivalent reflections from their mean, is given in table 2.

4. The magnetization distribution

This simple model of magnetization distribution used in the preliminary analysis was extended to allow anisotropy in the magnetization distribution at the B site using a multipole model. No

Table 2. Magnetic structure factors for $Fe_{72}Pt_{28}$ at 520, 300 and 100 K in μ_B/cell.

Fundamental reflections				Superlattice reflections			
	$T = 520$ K	$T = 300$ K	$T = 100$ K		$T = 520$ K	$T = 300$ K	$T = 100$ K
hkl	$H = 9.5$ T	$H = 9.5$ T	$H = 4.6$ T	*hkl*	$H = 9.5$ T	$H = 9.5$ T	$H = 4.6$ T
111	2.39(4)	4.28(13)	5.06(3)	100	−1.72(8)	−2.31(5)	−2.49(3)
200	2.06(7)	3.43(3)	4.38(8)	110	−1.36(6)	−1.95(2)	−2.103(9)
220	1.043(11)	1.834(12)	2.35(3)	210	−0.51(2)	−1.52(4)	
311	0.772(10)	1.35(5)	1.78(2)	211	−0.493(13)	−1.57(5)	
222	0.653(6)	1.17(2)	1.481(7)	221	−0.321(4)	−0.515(8)	
400	0.490(7)	0.847(11)	1.100(10)	310			−0.551(5)
331	0.268(5)	0.500(6)	0.647(9)	320	−0.254(4)	−0.43(2)	−0.453(15)
422	0.162(6)	0.286(6)	0.379(13)	321	−0.186(4)		−0.396(3)
511	0.139(10)	0.284(14)	0.374(5)	322			−0.285(7)
333	0.073(6)	0.151(9)	0.203(7)	410			−0.321(4)
440	0.054(8)	0.076(10)	0.111(7)	330	−0.075(2)	−0.187(4)	−0.21(2)
531		0.069(13)		411			−0.283(3)
442	0.001(7)	0.014(5)	0.022(7)	421			−0.188(5)
600		0.14(2)	0.19(1)	332	−0.052(2)	−0.129(8)	−0.154(2)
533	−0.018(9)	−0.048(10)	−0.061(9)	430	−0.049(4)	−0.109(8)	−0.118(13)
622		0.005(11)	0.011(8)	500			−0.11(3)
444	−0.039(9)	−0.084(11)	−0.104(5)	431			−0.107(11)
711		0.009(14)	0.032(6)	510			−0.135(2)
551	−0.029(12)	−0.064(10)	−0.090(7)	432			−0.067(10)
				521			−0.074(3)
				441			−0.031(4)
				550			0.024(8)

anisotropy was included for the A site for which the net magnetization is very small. In this model the magnetic structure factors $F_M(\mathbf{k})$ are given by

$$F_M(\mathbf{k}) = \mu_{Pt} r_A \langle j_0 \rangle_{Pt} + \mu_{FeA}(1 - r_A)\langle j_0 \rangle_{Fe} + r_B \sum_{i=1}^{i=3} \left(\sum_{L=0,2,4} \sum_{M=-L}^{M=L} \left(\langle j_L \rangle_{Fe} a_{LM} Y_L^M(\tilde{R}_i \hat{\mathbf{k}}) \right) + s\langle j_2 \rangle_{Fe} \right) \exp i\mathbf{k} \cdot (\tilde{R}_i \mathbf{r} + \mathbf{t}_i) \tag{6}$$

where the sum over i is over the three B sites generated by the symmetry operators $\tilde{R}_i : \mathbf{t}_i$ from the site at $\mathbf{r} = (\frac{1}{2}, \frac{1}{2}, 0)$ and the Y_L^M are linear combinations of spherical harmonic functions adapted to have the point group symmetry of the B sites ($4/mmm$). With this symmetry the degeneracy of cubic e_g functions is lifted giving independent x^2-y^2 and $3z^2-r^2$ orbitals, whilst the t_{2g} functions split into a doubly degenerate xz, yz pair and an independent xy function. The occupancies of these orbitals can be derived directly from the coefficients of the spherical harmonic functions in the structure factor expression of equation (6). As in equation (5) the magnetic scattering at the A site is the sum of the spherical Fe 3d and spherical Pt 5d form factors and the second term in the summation over i allows some flexibility in the radial part of the iron form factor. In the dipole approximation s represents the orbital moment of the iron atoms and a_{00} their total moment. The parameters in equation (6) were obtained by a least squares fit to the measured structure factors using the $\langle j_L \rangle$ form factors for a neutral iron atom. The results are given in table 3 and the percentage occupation of the different orbitals corresponding to these parameters in table 4.

Table 3. Parameters obtained from the least squares fits of equation (6) to the observed magnetic structure factors of $Fe_{72}Pt_{28}$.

Parameter	T (K) / H (T)	520 / 9.5	300 / 9.5	100 / 4.6
a_{00}		1.40(4)	2.37(7)	2.97(5)
a_{20}		0.10(2)	0.10(11)	0.03(2)
a_{44+}		0.07(2)	0.17(8)	0.13(4)
a_{40}		0.12(2)	0.10(7)	0.16(3)
s		0.10(2)	0.11(4)	0.13(3)
μ_{Pt}		0.07(10)	−0.44(18)	−0.26(32)
μ_{FeA}		−1.7(6)	−1.5(2.4)	1.4(1.2)
R		0.05	0.06	0.03

Table 4. Percentage occupancies of the different Fe 3d orbitals in $Fe_{72}Pt_{28}$.

T (K)	$x^2 - y^2$	$3z^2 - r^2$	Total e_g	xy	$zx + zy$	Total t_{2g}
100	23.6(1.1)	23.7(0.7)	47.3(1.3)	16.6(1.1)	36.1(1.0)	52.7(1.5)
300	24.1(3.7)	24.2(2.9)	48.3(4.7)	13.1(3.7)	38.5(3.4)	51.6(5.0)
520	21.4(1.6)	28.4(1.3)	50.0(2.0)	14.3(1.7)	36.0(1.8)	50.0(2.5)

5. Discussion

The results given in tables 3 and 4 show that there is no significant change in the relative numbers of unpaired electrons in the e_g and t_{2g} orbitals in $Fe_{72}Pt_{28}$ between 100 and 520 K. The small increase (2.7%) in e_g population is less than the experimental uncertainty. At the lower end of the temperature range the thermal expansion exhibits Invar behaviour and in the upper range normal Grüneisen behaviour. The results show that the magnetic carriers in the two regimes have essentially the same symmetry so the Invar effect cannot be due to thermal repopulation of states with significantly different orbital occupancies. These results are consistent with those obtained for the $Fe_{65}Ni_{35}$ Invar alloy [7]. It should nevertheless be pointed out that when the fractional occupation of e_g states is 50% it is not changed by transfer of majority spin t_{2g} electrons to minority spin e_g states. However, the parameter s which is sensitive to the radial extent of the B site form factor is also essentially independent of temperature. This again suggests that the electronic states occupied by the magnetic electrons change very little with temperature. It is also noteworthy that the fractions of electrons which occupy e_g orbitals in $Fe_{65}Ni_{35}$ and $Fe_{72}Pt_{28}$ are almost the same ($48 \pm 2\%$) in the two alloys. This is the largest e_g occupancy yet obtained for Fe in a 12-coordinated fcc environment, and probably represents the limit at which the fcc environment becomes unstable. The moments μ_A obtained for iron atoms at the A site are not reliable because, as was shown earlier, their value depends strongly on other assumptions made in the analysis. On the other hand, the platinum 5d moment μ_{Pt} depends only weakly on the model used. The results suggest that a Pt 5d moment of about 0.3 μ_B is aligned oppositely to the Fe atoms in the magnetically ordered state. No significant Pt moment is aligned in the paramagnetic state.

These results confirm the earlier finding that the explanation of the Invar effect based on a static interpretation of band structure calculations cannot be correct [7]. It must however be emphasized that these elastic scattering experiments do not probe correlations between the electronic configuration and the lattice vibrations. Other studies, including neutron inelastic neutron scattering, have shown that in $Fe_{72}Pt_{28}$ [10, 13] as in $Fe_{65}Ni_{35}$ [19, 14] such correlations

exist; they are manifest both in softening of the elastic constants and the TA $\{\zeta\,\zeta\,0\}$ phonons as well as in the appearance of additional magnetic excitations. All these data show that there is strong coupling between the magnetic degrees of freedom and the lattice and suggest that dynamic rather than static instabilities in the band structure drive the Invar effect.

Acknowledgments

We would like to thank H Bach and P Stauche, University of Bochum, for the preparation of the crystal and also E Lelièvre-Berna and E Bourgeat-Lami of the Institut Laue-Langevin for their support during the experiments on D3. Helpful discussions with E F Wassermann are gratefully acknowledged.

References

[1] Guillaume Ch E 1897 *C. R. Acad. Sci.* **10** 235
[2] Weiss R J 1963 *Proc. R. Soc.* **82** 281
[3] Kaspar J and Salahub D R 1981 *Phys. Rev. Lett.* **47** 54
[4] Williams A R, Moruzzi V L, Gelatt C D Jr, Kübler J and Schwarz K 1982 *J. Appl. Phys.* **53** 2019
[5] Moruzzi V l 1990 *Phys. Rev.* B **41** 6939
[6] Entel P, Hoffmann E, Mohn P, Schwarz K and Moruzzi V L 1993 *Phys. Rev.* B **47** 8706
[7] Brown PJ, Neumann K-U and Ziebeck K R A 2001 *J. Phys.: Condens. Matter* **13** 1563
[8] Sumiyama K, Masayuki S and Nakamura Y 1976 *J. Phys. Soc. Japan* **40** 996
[9] Tajima K, Endoh Y, Ishikawa Y and Stirling W G 1976 *Phys. Rev. Lett.* **37** 519
[10] Kästner J, Petry W, Shapiro S M, Zheludev A, Neuhaus J, Roessel Th, Wassermann E F and Bach H 1999 *Eur. Phys. J.* B **10** 641
[11] Ishikawa Y, Tajima K, Noda Y and Wakabayashi N 1980 *J. Phys. Soc. Japan* **48** 1097
[12] Rosov N, Lynn J W, Kästner J, Wassermann E F, Chattopadhyay T and Bach H 1994 *J. Appl. Phys.* **75** 6072
[13] Brown P J, Kanomata T, Matsumoto M, Neumann K-U and Ziebeck K R A 2002 *J. Magn. Magn. Mater.* **242–245** 781
[14] Brown P J, Roessli B, Smith J G, Neumann K-U and Ziebeck K R A 1996 *J. Phys.: Condens. Matter* **8** 1527
[15] Ito Y, Sasaki T and Mizoguchi T 1974 *Solid State Commun.* **15** 807
[16] Becker P J and Coppens P 1974 *Acta Crystallogr.* A **30** 129
[17] Freeman A J and Watson R E 1961 *Acta Crystallogr.* **14** 231
[18] Watson-Yang T J, Freeman A J and Koelling D D 1977 *J. Magn. Magn. Mater.* **5** 217
[19] Wassermann E F 1997 *The Invar Effect: a Centennial Symposium (Cincinnati, 1997)* ed J Wittenauer (Philadelphia, PA: The TMS Society) p 51